LAWRENCE
LIVERMORE
NATIONAL
LABORATORY

LLNL-JRNL-643260

The value of spatial information of for determining well placement: a geothermal example

W. J. Trainor-Guitton, G. M. Hoversten, A. Ramirez, J. Roberts, E. Juliusson, K. Key, R. Mellors

September 3, 2013

Geophysics

Disclaimer

This document was prepared as an account of work sponsored by an agency of the United States government. Neither the United States government nor Lawrence Livermore National Security, LLC, nor any of their employees makes any warranty, expressed or implied, or assumes any legal liability or responsibility for the accuracy, completeness, or usefulness of any information, apparatus, product, or process disclosed, or represents that its use would not infringe privately owned rights. Reference herein to any specific commercial product, process, or service by trade name, trademark, manufacturer, or otherwise does not necessarily constitute or imply its endorsement, recommendation, or favoring by the United States government or Lawrence Livermore National Security, LLC. The views and opinions of authors expressed herein do not necessarily state or reflect those of the United States government or Lawrence Livermore National Security, LLC, and shall not be used for advertising or product endorsement purposes.

The value of spatial information of for determining well placement: a geothermal example[1]

Whitney J. Trainor-Guitton[2], G. Michael Hoversten[3], Abelardo Ramirez[2], Jeffery Roberts[2], Egill Juliusson[4], Kerry Key[5] and Rob Mellors[2]

[1]LLNL-TBD
[2]Lawrence Livermore National Laboratory
7000 East Avenue
Livermore, CA, 94550, USA
e-mail: trainorguitton@llnl.gov

[3]ChevronTexaco
6001 Bollinger Canyon Rd.
San Ramon, CA 94583

[4]Landsvirkjun
Háaleitisbraut 68 • 103
Reykjavík, Iceland

[5]Scripps Institution of Oceanography
University of California San Diego
9500 Gilman Drive
La Jolla, CA 92093

Keywords: value of information, magnetotellurics, blind geothermal prospect

Abstract

Geophysical surveys improve upon simple well observations by providing spatial coverage. This provides information about geologic structure and can aid important decisions such as where to drill an additional well. We present a value of information (VOI) methodology designed specifically to aid these kind of decisions. We introduce an improvement from previous VOI methodologies by accounting for the effects of uncertainties associated with 2D geophysical inversion. VOI assesses the worth of information in terms of how it can improve the decision maker's likelihood of a higher-valued outcome. We demonstrate how VOI can be applied to spatial data using an exploration example for hidden geothermal resources. This methodology is applicable for spatial decisions for other exploration decisions (e.g. oil). We evaluate how well the magnetotellurics (MT) technique is able to delineate the lateral position of electrically

conductive materials that are indicative of a hidden resource. The conductive structure (referred to as the clay cap) represents where geothermal alteration has occurred.

We create prior earth models that include a clay cap in different lateral locations. We use these prior models to numerically simulate the data collection, noise, inversion and interpretation of the MT technique. MT's ability to delineate the correct lateral location can be quantified by comparing the true location in each prior model to what location was interpreted from each respective inverted model. We consider additional complexity in the earth models by adding more electrical conductors (not associated with the clay cap) and deeper targets. Both degrade the ability of the MT technique (the signal and inversion) to locate the clay cap thereby decreasing the VOI. Our results also demonstrate how VOI depends on whether or not a resource still exists below the clay cap, since the clay cap is only a potential indicator of economic temperatures.

Table 1: Table of Symbols

Clay cap location	x
Index of Clay Cap Locations	i
Total number of Considered Clay Cap Locations	N
Decision alternative	a
Existence or Non-Existence of Resource	θ
Value: metric to define outcome of decision	v
Vector of earth parameters	$\mathbf{z}$
Index of models with same clay cap location	t
Total number of realizations with clay cap i	T

Decision predictor/function (eg drilling)	$g_a(\cdot)$
Geophysical forward modeling (i.e. MT simulation)	$f(\cdot)$
Electrical resistivity model	ρ
Synthetic data	d
Synthetic data with noise	$\tilde{d}$
Inverted electrical resistivity model	$\tilde{\rho}$
Automatic interpretation function	$h(\cdot)$
Interpreted Location of Clay Cap	$\tilde{x}$
Index of interpreted Clay Cap Locations	j
Prior Value	Vprior
Value with Perfect Information	$V_{perfect}$
Value with Imperfect Information	$V_{imperfect}$
Value of Imperfect Information	$VOI_{imperfect}$

Introduction

Earth scientists inherently see the value of geophysical data; they appreciate that knowledge, although imperfect due to noise, the challenges of inversion, etc., is gained from the previous incomplete state of information. Geophysical surveys provide spatial coverage that sparse, expensive wells cannot. In many situations, however, it may be difficult to objectively quantify and demonstrate to decision-makers if knowledge has been (or can be) gained. A methodology known as value of information (VOI) objectively quantifies the value of a particular information source by appraising its relevance and reliability. VOI provides a metric that derives from the field of decision analysis and declares that an information source has value if it can improve a decision-maker's probability of making decisions with higher-valued outcomes (Howard, 1966; Pratt et al., 1995).

Bratvold et al. (2009) provides a review of the applications of VOI in the oil and gas industry, which includes some VOI demonstrations for geophysical data. Houck and Pavlov (2006) and Houck (2004, 2007) all use 1D reservoir models to evaluate the value of seismic amplitude data, controlled-source electromagnetics (CSEM) and 4D seismic data respectively. Pinto et al. (2011) evaluate the VOI of 4D seismic for two discrete reservoir cases. A very important shortcoming of these examples is that spatial variability and the associated uncertainty are not explicitly represented. In other words, the uncertainty modeling doesn't include different possible spatial distributions of reservoir parameters and how they would affect either the reliability of information from geophysical sources or the outcome of any exploration decision (i.e. where to drill).

Recently, spatial uncertainty has been included in VOI assessments of geophysical techniques. Eidsvik et al. (2008) used statistical rock physics models and spatial dependence within a VOI framework to decide whether or not to drill for oil. Spatial dependence is included in the 2D grids representing the porosity and saturation of the reservoir through a covariance model. At each of the grid locations, CSEM and seismic amplitude-versus-offset (AVO) data are drawn from likelihood models that represent the link between the reservoir properties and the geophysical attributes. Their method attempts to preserve spatial dependence through the spatially correlated porosity and saturation field. Bhattacharjya et al. (2010) present a VOI methodology for spatial decisions, where the spatial dependence of reservoir sands and shales are modeled as a Markov random field, and the value of seismic data is estimated for informing drilling decisions. Trainor-Guitton et al. (2011), Trainor-Guitton et al. (2013) and Trainor-Guitton et al. (2013) all include spatial uncertainty of aquifer properties for evaluating the VOI of different geophysical techniques for groundwater sustainability decisions. However, none of

these studies include multi-dimensional geophysical inversions and therefore, the uncertainties introduced by inversion haven't been included in the VOI assessment.

We present the first VOI methodology that includes the multi-dimensional nature of geophysical information with interpretation. This is significant as 2D or 3D inversion and interpretation make it possible for geophysical information to aid in spatial decision-making. A spatial decision can be defined as any decision whose outcome depends on the spatial distribution of some property (Trainor-Guitton, 2010). Our methodology recognizes that often the raw data from a geophysical source is not useful for spatial decisions; thus, the geophysical "information" will typically consist of the data, the inversion, and the interpretation in order to link the geophysical attributes to a parameter that would directly affect a decision outcome (e.g. a geologic horizon or unconformity). Here we present a VOI analysis that is applicable to decisions related to spatial exploration such as: "where to drill?"

Figure 1 graphically depicts the concepts behind VOI. Let's consider we are faced with some generic decision to most effectively exploit a subsurface resource (e.g. oil, minerals, gas, water, etc.) and the largest uncertainty is the resource's location. The horizontal axis from left to right represents lower to higher gains (utility or monetary returns) as outcomes from this generic decision. The lowest expected outcome (or calculated average) of the decision is shown to be when uncertainty is ignored (Figure 1a). For example, we could choose to disregard our ignorance (or our uncertainty) regarding the location of some subsurface resource. The next higher expected outcome (to the right) occurs when the current information and its uncertainty are accounted for when making the decision (Figure 1b). We will call this quantity the prior value: V_{prior}. Current information could represent the geologist's perspective on the likely locations of the resource. Next, we consider the highest expected outcome (furthest right oval:

Figure 1c), which is possible when "perfect information" is available before making our decision. We will call this quantity the value with perfect information: $V_{perfect}$. This concept conjectures that an infallible tool or information source exists such that it perfectly reveals (without errors or noise) the location of the sought-after resource. In other words, with perfect information, we will always place a well in exactly the right place to recover the resource.

By comparing $V_{perfect}$ (Figure 1c) and V_{prior} (Figure 1b), one can quantify if there is an increase in the expected outcome when making the decision with perfect information versus the current information. This potential increase is the value *of* perfect information: $\text{VOI}_{\text{perfect}}$. Therefore, in its simplest form, the VOI equation can be expressed as:

$$VOI = V_{with\ information} - V_{prior} \quad (1)$$

This expression makes some assumptions about the decision-maker's risk tolerance and utility function (Raiffa and Schlaifer, 1961). Value, *V*, is the metric used to quantify the outcome of a decision; the higher the value, the more "successful" an outcome of a decision is. Usually this is in monetary terms but it could also be in physical quantities (barrels of oil produced, BTU's produced, etc). The VOI of a particular technique in monetary terms can then be compared to the cost of acquiring that information; if the VOI greater than the cost, it is deemed a good decision to purchase that information.

The value with imperfect information ($V_{imperfect}$) is represented by the oval of Figure 1d. This quantity accepts that the "message" from the information source being evaluated (e.g. seismic, controlled source EM) will not always accurately identify the location of the resource. Therefore, this quantity is depicted as lower-valued (to the left in Figure 1) compared to the value with perfect information ($V_{perfect}$: Figure 1c). The value **of** imperfect information,

$VOI_{imperfect}$, can be quantified by comparing it to V_{prior}. In other words, if you can account for the inaccuracies of the information source and demonstrate that it would still increase the expected outcome over a decision made with the current information, the imperfect information will be deemed valuable (Equation 1).

In order to obtain a $V_{imperfect}$ measure, one must estimate the reliability of the information source. Bratvold et al. (2009) describe how quantitative methods are needed to evaluate the information reliability. We will consider the reliability of the geophysical source to spatially resolve a resource target. Our approach includes the effects of the inversion image resolution and its impact on the information reliability. Therefore, we include spatial uncertainty in the VOI methodology thereby improving the VOI metrics used for exploration decisions.

Hidden Geothermal Resource

We demonstrate our spatial VOI methodology using a hypothetical geothermal exploration example. We suggest that our methodology is transferable to other applications. Our example is motivated by Cumming (2009) who conceptualized hidden (or blind) geothermal resources. Figure 2 demonstrates a possible blind/hidden geothermal resource where no surface expression exists to indicate a possible geothermal resource. His model (Figure 2) demonstrates a scenario where faults and fractures allow for the circulation of hot water to accessible depths. As a result, smectite and illite clays are formed just above the shallowest depths where the hot water circulates.

Similar to oil exploration, the geothermal community has employed geophysical surveys to characterize the subsurface with to improve its knowledge of subsurface reservoirs and to reduce their exploration risks. DC electrical resistivity and self-potential techniques have been

employed to decipher potential flow paths for hot water (Richards et al., 2010), whereas micro seismic travel times (Wu and Lees, 1999) and magnetotellurics (MT) data (Garg et al., 2007; Newman et al., 2008) have been used to infer the 3D geologic structure of geothermal areas.

Also like oil exploration, geothermal prospecting with geophysical techniques is complicated by challenges related to the non-unique relationship of geophysical attributes in the subsurface and the geothermal reservoir parameters. Historically, the MT technique has been used to delineate zones of low resistive materials that can be indicative of alteration caused by the circulation of hot fluids (Gunderson et al., 2000). This alteration is often referred to as the clay cap; we adopt this terminology here. However, low resistivity zones can also be created by the presence of brines and/or clay-rich sediments (Newman et al., 2008; Ucok et al., 1980). Another complicating factor is that the clay cap alteration reflects the historical high temperature of the system. Therefore, the existence of clay cap does not ensure that economic temperatures still exist below it. Karlsdóttir et al. (2012) describe how the resistivity alone cannot confirm a viable geothermal resource:

> *The resistivity reflects the alteration caused by the heating of the rocks and reflects the peak temperature experienced by the system, being it at the present or in the past. … The resistivity structure reflects the temperature, provided there is equilibrium between alteration and present temperature. In case of cooling the alteration may remain and the resistivity will reflect the temperature at which the alteration was formed. Whether the resistivity (and the alteration) indicates the present temperature of the system will only be confirmed by drilling.*

Information Source considered: Magnetotellurics

MT has strengths and weaknesses when used to explore for geothermal resources. Figure 3, also from Cumming (2009), provides a conceptual model of electrical resistivity for the geologic representation of Figure 2. The hidden resource is at the apex of the isotherms which coincides with the concave-side of the 10 ohm-m clay cap (yellow). Therefore, for our modeling and VOI demonstration purposes, this clay cap (yellow) is the key ***potential*** indicator of the resource.

The MT measurements may help us determine where a clay cap exists, but they can't tell us definitively about the temperature below the cap. Additionally, the cap's lower electrical resistivity tends to shunt electrical currents and greatly reduces sensitivity to the properties of the deeper reservoir properties. The VOI method described here will allow us to quantify both MT's usefulness (spatial coverage and sensitivity to low resistive clays) and limitations (low resistivity is not uniquely associated with higher temperature, i.e. whether a resource exists or not).

Thus, the work presented here will use this geothermal example to demonstrate a spatial VOI methodology. The next section (Problem Description) describes how the prior uncertainty of the subsurface (i.e. the state of knowledge before the MT survey data is available) is represented with simplified geothermal reservoir models that represent different possible locations of the resource. The next section will also describe V_{prior} , which captures the expected outcome of a decision taken without the benefit of MT data. In the Methodology section, we devise a method for estimating MT's reliability to determine the location of the geothermal reservoirs. This step involves simulating the MT response using the prior models and inverting this data to construct electrical resistivity images. This section also describes how the value with imperfect information ($V_{imperfect}$) is calculated using the reliability. The Results section presents

the value of imperfect information results for several different reliabilities and priors, along with complexities added to the prior models. Through the decision uncertainty and the models included in the prior, we will demonstrate how VOI can underscore the strengths and weakness of a particular information source.

Problem Description: Uncertainty of Possible Hidden Resource (Clay Cap) Location and Where to drill?

Figure 4 shows a decision tree that depicts the decision scenario that we have described. The tree represents the decision-to-outcome process chronologically from left to right. First a decision of where to drill is taken (extreme left). The final outcome (extreme right) will depend on where the clay cap is and if a resource exists under the cap. For this work, we only consider how the MT source can help detect the location of the clay cap. In the Results Section, we will introduce how we account for the probability of the resource existing (represented by $Pr(\Theta = \theta_k)$) given the existence of the clay cap.

To represent our uncertainty in the location of the clay cap, we create prior models with clay caps of varying lateral locations. We assume the hidden resource below the clay cap can only exist in one of *N* discrete locations. Within our prior models, the clay cap is represented at *N*=15 different locations, where the horizontal location (x) of the middle of the clay cap varies between -3500m and +3500m. Let us represent each model by

$$\boldsymbol{z}^{(t)}(X = x_i) \quad i = 1, \dots, N \tag{2}$$

where vector ***z*** contains the electrical resistivity and any other relevant properties (i.e. temperature, porosity, etc.) of the model. Initially, we assume that the low electrical resistivity of

the clay cap is equivalent to higher temperatures and higher permeability thanks to faults and fractures shown in Figure 2. Figure 5 demonstrates model $\boldsymbol{z}^{(t)}(X = 0)$; the variable x identifies the location of the "throat" of the clay cap. Figure 3 portrays this "throat" as the shallowest location with the highest isotherm. Therefore, the x_i location represents the shallowest access to the potential resource. The clay cap in all models ranges between 0.5 and 1.5 km depth and is 3km wide.

We assume that one can only consider drilling in these N locations, if at all. Thus, the spatial alternatives (represented by index a in Figure 4) consist of N possible clay cap locations where one may choose to drill or not. These are represented as the columns in Table 2, while the different possible clay cap locations (model categories x_i) are represented by the rows of Table 2. The last column of the table represents the option to not drill at all.

Table 2: Table of Decisions alternatives (a) and value outcomes (v) assuming resource exists under clay cap

Alternatives → Clay Cap Locations (in models) ↓	Drill @ x=+3500m (a=1)	Drill @ x=+3000m (a=2)	…	Drill @ x= -3000m (a=14)	Drill @ x= -3500m (a=15)	Don't Drill (a=16)
Clay Cap @ x= +3500m	**Highest Value $$**	**Value $**	…	**LOSS**	**LOSS**	0
Clay Cap @ x= +3000m	**Value $**	**Highest Value $$**	…	**LOSS**	**LOSS**	0
⋮				⋮	⋮	⋮
Clay Cap @ x= -3000m	**LOSS**	**LOSS**	…	**Highest Value $$**	**Value $**	0
Clay Cap @ x= -3500m	**LOSS**	**LOSS**	…	**Value $**	**Highest Value $$**	0

The outcome of choosing a decision alternative a with a clay location of x_i, is quantified with the "value outcome metric." The value metric allows for comparison between outcomes from different decision alternatives, which can be represented by function g_a.

$$v_a(x_i) = g_a\big(z(\mathrm{X} = x_i)\big) \tag{3}$$

$$a = 1, .., N+1 \quad i = 1, \dots, N$$

Table 2 shows that the highest outcomes (most successful decisions) occur along the diagonal: when the drilling location aligns with the actual location of the middle of the clay cap. The value outcomes then drop off as you move away from the diagonal signifying the mismatch between the possible resource location and the drilling location.

V_{prior}: the best decision option given the prior uncertainty

Decision analysis concepts are often described in terms of lotteries and prizes (Pratt et al, 1995). By choosing to drill or not, a decision maker is choosing whether or not to participate in a lottery with certain perceived chances of winning a prize (drilling into a profitable reservoir); however, this lottery also involves the chances of losing money (missing the resource or drilling into an uneconomic reservoir). By utilizing V_{prior}, a decision-maker can logically determine when one should participate in this lottery given both the prior uncertainties and possible gains and losses.

V_{prior} is only dependent on the current state of uncertainty ($Pr(X = x_i)$) and the outcomes of the decision ($v_a(x_i)$):

$$V_{prior} = \max_a \left(\sum_{i=1}^{N} Pr(X = x_i) v_a(x_i) \right) \; a = 1, \dots, N+1 \tag{4}$$

The V_{prior} expression identifies which decision alternative will on average result with the highest value (most successful outcome). The prior distribution is used to calculate a weighted average inside the summation and the **max** finds the highest outcome value among all the different spatial alternatives a.

a

V_{prior} is inherently a very subjective measure since the prior state of knowledge is usually characterized by an unknown probability distribution. Therefore, we test three different prior distributions and two different value outcome matrices (Table 2) and how they affect the final $VOI_{imperfect}$. Figure 6 displays the three prior distributions. The uniform distribution (solid line) declares that there's an equal likelihood that the clay cap exists at any of the *N* locations between -3,500m and +3,500m. The two Gaussian distributions (dashed and dotted curves in Figure 5) reflect a belief that the resource is centered at x=0. The Gaussian with the smaller standard deviation (dotted curve) reflects less uncertainty of the location than the Gaussian with the larger standard deviation (dashed curve).

Two different value outcome matrices are used to compare their influences $VOI_{imperfect}$. Figure 7 displays a value outcome matrix that penalizes drilling decisions that miss the clay cap by ≥1500m. Alternatively, Figure 8 is a more "forgiving" value outcome matrix, in that losses are not incurred until the drilling location is farther (≥2,000m) from the actual location of the clay cap. The individual values in Figure 7 and Figure 8 are arbitrary and can be replaced by more realistic dollar amounts in order to represent specific locations or particular drilling applications.

Table 3 contains the resulting six different V_{prior}*'s* using the value outcomes of both Figure 7 and Figure 8. The prior uncertainty of the location of the clay cap decreases down the rows of the Table 3 and the overall individual value outcomes are greater in the furthest right column. Therefore, V_{prior} is lowest in the top left and highest in the bottom right of the table. This makes sense because the uniform distribution describes a completely uninformative prior. Therefore entering the "geothermal lottery" is quite risky. However, if the uncertainty of the clay

cap location decreases (represented by the Gaussian distributions) then the V_{prior} increases, particularly with a smaller standard deviation (last row). These Gaussian distributions could represent a situation where prior geological or well information exists that indicates a possible clay cap location. The last column uses the individual value outcomes that drop-off more slowly for increasing mismatches between the drilling and the clay cap locations (the off-diagonals of Table 2). Therefore, there is less risk of a monetary loss for the right column and all the V_{prior}'s are higher in this column.

Table 3: Vprior for different prior uncertainties (rows) and different individual value outcomes (columns).

Prior Distribution ↓	$v_a(x_i)$**: Gains drop quickly (Figure 7)**	$v_a(x_i)$**: Gains drop off slowly (Figure 8)**
Uniform Prior	$0	$0
Gaussian Prior (μ=0m, σ^2=1800)	$0	$50,276
Gaussian Prior (μ=0m, σ^2=900)	$109,534	$293,603

$V_{perfect}$: Value with perfect information

The value of perfect information ($VOI_{perfect}$) provides an upper bound the utility benefits that a given information source could offer, given the prior uncertainties and modeled value outcomes. Perfect information for this example assumes that some measurement could reveal without error, the location of the clay cap. Theoretically, one would drill exactly at the neck of the clay cap with this perfect information. The value with this perfect information is expressed as

$$V_{perfect} = \sum_{i=1}^{N} Pr(X = x_i) \left(\max_a v_a(x_i) \right) \; a = 1, \dots, N+1 \qquad (5)$$

which only differs from V_{prior} by the placement of the **max** (**a**), which is now before the averaging operation: ($\sum_{i=1}^{N} Pr(X = x_i)$). Equation 5 suggests that we will have the information before we

choose a location for drilling (a), and therefore we can choose the alternative that has the highest value for each clay cap location. For both value outcome matrices (Figures 7 and 8), this is the value along the diagonal: $500,000. Then the average of all best outcomes for each of the clay cap locations is calculated. Since all three of the prior distributions are symmetric, $V_{perfect}$ is $500,000 for all 6 combinations of prior uncertainty distributions and value outcomes (Table 4). Following Equation 1 (depicted graphically in Figure 1), the value *of* perfect information, is the difference between this and V_{prior}.

$$VOI_{perfect} = V_{perfect} - V_{prior} \quad (1)$$

As seen in Table 4, information has the most value ($500,000) when the prior uncertainty is high (both the uniform prior and wider Gaussian) and when greater losses are experienced when one drills far from the target (Figure 7). Again, this is logically intuitive from the viewpoint of the decision-maker.

Table 4: $VOI_{perfect}$ for different prior uncertainties (rows) and different individual value outcomes (columns

Prior Distribution ↓	**$v_a(x_i)$: Gains drop quickly (Figure 7)**	**$v_a(x_i)$: Gains drop off slowly (Figure 8)**
Uniform Prior	$500,000 - $0 = $500,000	$500,000 - $0 = $500,000
Gaussian Prior (μ=0m, σ^2=1800)	$500,000 - $0 = $500,000	$500,000 - $50,276= $449,723
Gaussian Prior (μ=0m, σ^2=900)	$500,000 - $109,534 = $390,465	$500,000 - $293,603= $206,396

Methodology: Simulating MT Data Collection, Noise, Inversion and Interpretation of Clay Cap Location

The positive $VOI_{perfect}$ results indicate that a new source of information could have value. However, as indicated in Figure 1, once we consider a specific source of information and include

its inaccuracies in locating the clay cap, the value of imperfect information ($VOI_{imperfect}$) will be less than $VOI_{perfect}$. For this demonstration, we want to assess the value of the magnetotellurics (MT) geophysical technique. Consequently, we must have an estimate of MT's reliability to locate the clay cap. We estimate the reliability by mimicking the data collection, inversion and interpretation processes. Specifically, we simulate the physics of the MT measurement on many geothermal reservoir models that represent possible exploration scenarios, corrupt the data to simulate measurement error, and then perform inversions of noisy MT data. Lastly, we interpret from the resulting resistivity images the location of the clay cap.

The workflow to estimate the value with imperfect MT information can be described in 7 steps.

1. The MT response for each prior model is predicted using the electromagnetic simulation MARE2DEM (Key and Ovall, 2011). The forward response is represented by function $f(\cdot)$ and the dataset for each prior model by d_i.

$$d_i = f\big(\boldsymbol{z}(x_i)\big) \quad i = 1 \ldots, N \tag{6}$$

   Frequencies between 0.001 and 1000 Hz (21 frequencies total, 3-4 per decade) are observed at 21 receiver locations. The line of MT receivers covers -5,000m to +5,000m. Therefore for all *N* locations, the entire clay cap is covered.
2. 4% random Gaussian noise is added to all of the *N* (each of the prior models) MT forward responses. Different seeds are used to generate different random noise. *t* indexes the different "realizations" of noise, which is added to the same forward response. Therefore *T*N* noisy datasets are generated.

$$\tilde{d}_i^{(t)} = d_i + 0.04 d_i^{(t)} * N(0,1) \quad i = 1 \dots, N \;\; t = 1, \dots, T \tag{7}$$

3. Geophysical inversions are performed using the *T*N* noisy data set; *T=5* inverted electrical resistivity models ($\tilde{\rho}_i^{(t)}$) are obtained for every prior model (justification for T=5 will be explained in step 4). Figure 9 includes 3 prior models (first column) and their respective inversion models (last column).

$$\tilde{\rho}_i^{(t)} = f^{-1}\left(\tilde{d}_i^{(t)}\right) i = 1 \dots, N \;\; t = 1, \dots, T \tag{8}$$

4. For each inversion result, we use an automatic interpretation algorithm (denoted by function $h(\cdot)$) to locate the clay cap "throat" at 5 depth locations (represented by index *k*) spanning the thickness of the 500m clay cap neck. Therefore, for each inversion image, an interpretation of the lateral location of the clay cap neck is made at the following depths: {1.1, 1.2, 1.3, 1.4, 1.5}km. Figure 10 shows the automatic picks at these depths for one example inversion image; these picks are represented by $\tilde{x}_j^{(t,k)}$.

$$\tilde{x}_j^{(t,k)} = h\left(\tilde{\rho}_i^{(t)}\right) \;\; i, j = 1 \dots, N \;\; t = 1, \dots, T \; k = 1, \dots, K \tag{9}$$

The lower resistivity region ($\tilde{\rho}$ <$10^{1.7}$ or 50 Ohm-m; the darker colors of Figure 10) represents the clay cap or alteration. Therefore, the interpreted clay cap "throat" locations, $\tilde{x}_j^{(t,k)}$, are the lateral locations of maximum resistivity (representing the apex of the isotherm) within this lower resistivity region. This interpretation algorithm allows for different lateral locations to be chosen at the 5 fixed depths given above. This is a

significant assumption that the depths are known. Future work, will improve this algorithm to allow for uncertainty in the depth interpretation.

A test inversion was run for *T=15* for $\boldsymbol{z}(x_i = 0)$, and the statistics of the interpretations $\tilde{x}_j$ were comparable for *T=5* (i.e., the mean and variance of the interpretations were the same).

5. The data likelihood/reliability is calculated by comparing the interpreted location of clay cap in the inverted image ($\tilde{x}_j{}^{(t)}$) to its prior model's original location ($x_i{}^{(t)}$).

$$Pr\left(\tilde{X} = \tilde{x}_j{}^{(t,k)} | X = x_i\right) \quad i,j = 1 \dots, N \; t = 1, \dots, T \; k = 1, \dots, K \qquad (10)$$

6. We then use Bayes rule to estimate the probability of the actual clay cap location given an interpreted clay location $\tilde{x}_j{}^{(t)}$. This is the information posterior distribution.

$$Pr\left(X = x_i | \tilde{X} = \tilde{x}_j{}^{(t,k)}\right) \quad i,j = 1 \dots, N \; t = 1, \dots, T \; k = 1, \dots, K \qquad (11)$$

How the reliability and information posterior are calculated will be further explained later in this section.

7. Lastly, the value with imperfect information ($V_{imperfect}$) is calculated using the information posterior.

$$V_{imperfect} = \sum_{j=1}^{J} \Pr\left(\tilde{X} = \tilde{x}_j\right) \left\{ \max_a \left[\sum_{i=1}^{15} Pr\left(\mathrm{X} = x_i | \tilde{X} = \tilde{x}_j\right) v_a(x_i) \right] \right\} \qquad (12)$$

$$a = 1, \dots, N+1$$

Table 5 is one way to visualize the information posterior calculated in Step 6 (Equation 11). The rows represent the actual or true clay cap location and the columns represent the

interpreted locations. The frequency (count per each row-column combination) is calculated and used in the value with imperfect information ($V_{imperfect}$) expression (Equation 12). The sum of each column will be 1.

Table 5: Information content of MT to decipher location of clay cap.

Interpreted locations→ **True locations ↓**	**Interpret Clay Cap at x=+3500m (j=1)**	**Interpret Clay Cap at x=+3000m (j=2)**	**…**	**Interpret Clay Cap at x= -3500m (j=N)**
Clay Cap @ x= +3500m (i=1)	$Pr(\mathrm{X} = \mathrm{x_{i=1}} \mid \tilde{X} = \tilde{x}_{j=1})$	$Pr(\mathrm{X} = \mathrm{x_{i=1}} \mid \tilde{X} = \tilde{x}_{j=2})$	…	$Pr(\mathrm{X} = \mathrm{x_{i=1}} \mid \tilde{X} = \tilde{x}_{j=N})$
Clay Cap @ x= +3000m (i=2)	$Pr(\mathrm{X} = \mathrm{x_{i=2}} \mid \tilde{X} = \tilde{x}_{j=1})$	$Pr(\mathrm{X} = \mathrm{x_{i=2}} \mid \tilde{X} = \tilde{x}_{j=2})$	…	$Pr(\mathrm{X} = \mathrm{x_{i=2}} \mid \tilde{X} = \tilde{x}_{j=N})$
⋮				
Clay Cap @ x= -3500m (i=N)	$Pr(\mathrm{X} = \mathrm{x_{i=N}} \mid \tilde{X} = \tilde{x}_{j=1})$	$Pr(\mathrm{X} = \mathrm{x_{i=N}} \mid \tilde{X} = \tilde{x}_{j=2})$	…	$Pr(\mathrm{X} = \mathrm{x_{i=N}} \mid \tilde{X} = \tilde{x}_{j=N})$

The value with imperfect information $V_{imperfect}$ (Equation 12) uses the information posterior as a "misinterpretation rate:" accounting for how frequently the interpretation of the MT images may correctly or incorrectly locate the clay cap. With this interpretation of the clay location $\tilde{x}_j$ from the information, the alternative with the highest outcome can be selected ($\mathbf{\max_{a}}$ in Equation 12)**.** This is calculated for every possible interpretation (index j) and these are weighted by the data marginal, $\Pr(\tilde{X} = \tilde{x}_j{}^{(t,k)})$, which accounts for how often that interpretation may occur.

The asymmetry of the true clay cap structure should be noted here as it affects the inversion, interpretation, and ultimately the calculated information posterior. Notice in Figure 5 how the neck of the clay cap is centered to the west (left) of structure. The center of mass of all the models is 350m to the east (right) of the centerline of neck location.

With this in mind, the information posterior values for this example, shown in Figure 11, are reasonable: a visual bias of misinterpretations is seen to the right of the diagonal representing that the neck is interpreted to the east its actual location. In this example, the inversion and interpretation of the MT data indicate that clay caps at x= -3,000m and x= -1,000m will always be correctly located; this is indicated by the 100% in the diagonal. Interpretations from inversions for all other locations will produce some erroneous locations.

Two $V_{imperfect}$ measures can be calculated using the two value outcome matrices of Figure 7 and 8. These are shown **in the first row** Table 6 (the 2nd and 3rd row display $V_{imperfect}$ for results explained in the next section). As expected (see conceptual graphic in Figure 1), both of these $V_{imperfect}$'s are lower than $V_{perfect}$ of $500,000 (Equation 5). Also, $V_{imperfect}$ is lower when the less "forgiving" value outcome matrix (Figure 7) is used. When the interpreted location doesn't match the actual location, this matrix will create larger losses and consequently a lower $V_{imperfect}$ compared to the case when Figure 8 is used.

Table 6: $V_{imperfect}$ results two different value outcome matrices (Figures 7 and 8) and different prior models (rows).

	$v_a(x_i)$: Gains drop quickly (Figure 7)	$v_a(x_i)$: Gains drop off slowly (Figure 8)
$V_{imperfect}$: Clay Cap only	$368,533	$436,394
$V_{imperfect}$: Clay Cap & Sinter	$350,133.	$432,464
$V_{imperfect}$: Deeper Clay Cap & Sinters to the East	$167,022	$268,261

Results: Value of Imperfect Information

Now the value *with* imperfect information, $V_{imperfect}$, can be put into the VOI equation (Equation 1) to calculate the value *of* imperfect information $VOI_{imperfect}$:

$$VOI_{imperfect} = V_{imperfect} - V_{prior} \quad (13)$$

Six different $VOI_{imperfect}$'s are calculated using the previous V_{prior} (Table 3) and the two $V_{imperfect}$'s (Table 6). These are shown in Table 7. The value of imperfect information is highest ($436,394) when the prior uncertainty of the clay cap location is highest (uniform prior and Gaussian with σ^2=1800) and the penalties for drilling far from the clay cap are more forgiving (Figure 8). Information from MT should have more value when our ignorance is highest and the risk for costly outcomes from decisions is greater. However, once the fallibility of the MT technique is considered, the final VOI depends on both $V_{imperfect}$ and V_{prior}. As seen in Table 7, $VOI_{imperfect}$ is higher for the more forgiving outcomes; this is because misinterpretations are punished less for this value matrix. Conversely, the value of imperfect information is lowest ($142,790) when the V_{prior} is greatest (Gaussian with σ^2=900) and drilling farther from the actual clay cap results in a smaller economic loss.

Table 7: $VOI_{imperfect}$ results for models with clay caps only

$VOI_{imperfect}$	$v_a(x_i)$: Gains drop quickly (Figure 7)	$v_a(x_i)$: Gains drop off slowly (Figure 8)
Uniform Prior	$368,533 - $0 = $368,533	$436,394 - $0 =$436,394
Gaussian Prior (μ=0m, σ^2=1800)	$368,533 - $0 = $368,533	$436,394 - $50,276 =$386,118
Gaussian Prior (μ=0m, σ^2=900)	$368,533 - $109,534 = $258,998	$436,394 - $293,603 = $142,790

Adding complexity to the prior models: the conductive, inactive sinter

We repeat the workflow described in Section 3, but we add some complexity to the prior models. Figure 12 depicts an inactive sinter above and to the east of the clay cap (the orange-colored feature). Sinters are a siliceous or calcareous deposit precipitated from mineral springs,

and in Figure 3 (Cumming, 2009) it is hypothesized to have a lower resistivity (5 Ohm-m) than that of the clay cap (10 Ohm-m).

The sinter will impact the inversions and more importantly the interpretation of where the neck of the clay cap is. Figure 13 is the inversion result of Figure 12. We see that the MT image indicates the presence of the low resistivity sinter but does not perfectly resolve its location. If we compare it to the inversion result without the sinter (Figure 9), we see that the area of lower resistivity (warmer colors) has now shifted to the east (right) due to the sinters location.

MT inversions and interpretations are performed for models including a sinter at all N=15 locations as explained in Section 3. Then, the information posterior (shown in Figure 14) is calculated using prior models that include this sinter. If we compare it to the information posterior from models with no sinter (Figure 11), we see a visible shift from the diagonal to the right. Recall how the automatic interpretations are made: the location of the maximum resistivity is chosen from within the minimum resistivity region (representing the clay cap or alteration). Therefore, since the minimum resistivity region (the "warm colors area") has shift east (right), the interpreted clay cap "throat" location has now shifted east (right). The other significant difference is seen in the column of interpreted location $\tilde{x}_j = -3{,}000m$. This column indicates that none of the interpretations resulted in a throat at $\tilde{x}_j = -3{,}000m$. This will be reflected in the data marginal: $\Pr(\tilde{X} = -3{,}000m) = 0$.

$V_{imperfect}$ (Equation 12) is calculated using this information posterior from the models with sinters and the two value outcome matrices. These are shown in the second row of Table 6. $V_{imperfect}$ has decreased for both value outcomes (columns of Table 6) compared to the cases

where only the clay cap was modeled (row 1 of Table 6). This is what one would expect given the visible shift in the information posterior which includes the effect of the sinter (Figure 14). The subsequent $VOI_{imperfect}$ for three different V_{priors} are shown in Table 8.

Table 8: $VOI_{imperfect}$ results for models with clay cap and sinters.

$VOI_{imperfect}$	$v_a(x_i)$: Gains drop quickly (Figure 7)	$v_a(x_i)$: Gains drop off slowly (Figure 8)
Uniform Prior	$350,133 - $0 = $350,133	$432,464- $0 = $432,464
Gaussian Prior (μ=0m, σ^2=1800)	$350,133- $0 = $350,133	$432,464- $50,276 = $382,187
Gaussian Prior (μ=0m, σ^2=900)	$350,133 - $109,534 = $240,598	$432,464 - $293,603= $138,860

Deeper targets: dipping eastward clay cap

Suppose that the prior geological information postulates that if a clay cap exists in the eastern part of the considered location, it will be deeper than if it is in the extreme west. This could be due to many different geological scenarios, such as local variations in mineralogy which cause the fractures to plug fractures more in the east than the west, causing the clay cap to form deeper. Or perhaps the uplift regime would give reason to expect shallower clay caps to develop in the west. Figure 15 graphically demonstrates how the clay cap will be incrementally deeper with increasing eastern location. In our example, the clay cap and sinter are placed 100m deeper every 500m to the east.

At x= -2,500m the model is 200m deeper than its original location, and at x= +2,500m the model is 1,200m deeper than its original location. The top row of Figure 16 shows the inversion results for the clay cap and sinters of these two lateral locations at their original depths. The second row shows the inversion results for these same lateral locations but for the two increased depths. Even for -2,500m (only 200m deeper) we see that the MT inverted image does

recover electrical resistivities lower than 10 ohm-m. The second column shows that the 1,200m deeper clay cap and sinter is not resolved at all.

In fact, the automatic interpretation does not identify any area of lower resistivity for clay cap's at $x_i \geq$ +2,500m. We account for this in the information posterior in the following way. We assume that for $x_i = \{+2{,}500\text{m};\ +3{,}000\text{m};\ 3{,}500\text{m}\}$ an interpretation x_j is equally likely at any of the *N* particular lateral locations: $Pr(\tilde{X} = \tilde{x}_j \ \ |X = x_i) = \frac{1}{N}$. This is then carried over into the information posterior, such that every interpretation has some probability of actually representing clay cap locations of $x_i = \{+2{,}500\text{m};\ +3{,}000\text{m};\ 3{,}500\text{m}\}$.

Figure 17 illustrates the information posterior for these dipping clay cap and sinters. Only four diagonal locations have non-zero probability (not including $x_i = \{+2{,}500\text{m};\ +3{,}000\text{m};\ 3{,}500\text{m}\}$ since no interpretation could be made from these inversions). Recall that the diagonal represents the frequency at which a correct clay cap location is made from the interpretation of the inversion image. Compare this to 12 non-zero diagonal probabilities for the original case where no sinter existed. The largest difference in the information posterior relative to the two others, is the probability of a clay cap to truly be located at one of the three most eastern and deepest clay caps ($x_i = \{+2{,}500\text{m};\ +3{,}000\text{m};\ 3{,}500\text{m}\}$) given *any* of the interpretations ($x_j\ \forall j$). This is a result of the inability of the MT technique to resolve the three deepest clay caps.

Table 9 contains the $VOI_{imperfect}$ results for the clay cap and sinters with varying depths. These $VOI_{imperfect}$ values are much less than the previous values (Table 7 and Table 8). $VOI_{imperfect}$

= 0 for this case when the prior uncertainty is the least (μ=0m, σ^2=900) and smaller economic losses are expected.

Table 9: $VOI_{imperfect}$ results for models with clay cap and sinters that have increasing depth to the east.

$VOI_{imperfect}$	$v_a(x_i)$: Gains drop quickly (Figure 7)	$v_a(x_i)$: Gains drop off slowly (Figure 8)
Uniform Prior	$167,022 - $0 = $167,022	$268,261- $0 = $268,261
Gaussian Prior (μ=0m, σ^2=1800)	$167,022 - $0 = $167,022	$268,261- $50,276 = $217,984
Gaussian Prior (μ=0m, σ^2=900)	$167,022 - $109,534 = $57,487	$268,261- $293,603 = $0

Accounting for no resource under clay cap

Up until now, we have made a very significant assumption that a resource does exist under the clay cap: $Pr(\Theta = \theta_{k=1}) = 1$. Now we will account for the probability of no resource existing under the clay cap. This is represented as the second uncertainty in the decision tree of Figure 4. We link each combination of prior model and decision alternative to two possible value outcomes: the value outcome if there is a resource ($\theta_{k=1}$) or not ($\theta_{k=0}$). The average of the two now replaces the quantity of Equation 3:

$$v_a^{(t)}(x_i) = Pr(\Theta = \theta_{k=0})\, v_a^{(t)}(\theta_{k=0}) + Pr(\Theta = \theta_{k=1}) v_a^{(t)}(\theta_{k=1}) \qquad (14)$$

$$a = 1, \dots, N+1 \;\; i = 1, \dots, N$$

where $Pr(\Theta = \theta_{k=1,2})$ is the probability of an economic resource existing under the clay cap. For now, we assume that the resistivity structure would remain the same whether a resource exists or not under the clay cap since the clay cap is representative of the historical temperature (see Section 1). Table 10 demonstrates how the value of information decreases with decreasing probability of occurrence of an economic reservoir.

Table 10: $VOI_{imperfect}$ for different probabilities of an economic resource occurring under the clay cap.

$VOI_{imperfect}$ $v_a(x_i)$: Gains drop quickly (Figure 7)	**$Pr(\theta = \theta_{k=1})$ = 1.0**	**$Pr(\theta = \theta_{k=1})$ = 0.7**	**$Pr(\theta = \theta_{k=1})$ = 0.5**	**$Pr(\theta = \theta_{k=1})$= 0.3**
Uniform Prior	$368,533 - $0 = $368,533	$167,973 - $0 = $167,973	$34,266 - $0 = $34,266	$0 -$0 = $0
Gaussian Prior (μ=0m, σ^2=1800)	$368,533 - $0 = $368,533	$167,973 - $0 = $167,973	$34,266 - $0 = $34,266	$0 -$0 = $0
Gaussian Prior (μ=0m, σ^2=900)	$368,533 - $109,534 = $258,998	$167,973 - $0 = $167,973	$34,266 - $0 = $34,266	$0 -$0 = $0

Conclusions and Discussion

Our results show how the value of information depends on four factors. We identify these conclusions and discuss the limitations of how each was presented in this work.

The reliability of the information from MT: data, inversion & interpretation

If we compare Table 4 to either Table 7, Table 8 or Table 9, we see the impact of the "imperfect MT images." Because of inaccuracies introduced from the added noise, inversion, interpretation, and MT's limited resolution, we won't always perfectly identify the clay cap's location. We account for this by estimating MT's reliability (and in turn the information posterior) and calculating the value of imperfect information ($VOI_{imperfect}$). First, the inversion technique uses a regularization scheme based on minimum roughness to stabilize the inversion. This approach produces smooth images where the structural features are smeared and accurate shape information is lost. Second, MT's ability to resolve the throat of the clay cap was diminished when a conductor of 5 ohm-m (representing a possible sinter) was included. Third, the information posterior reflected increased inaccuracy when the depth of the structure (clay cap) was increased incrementally. This is consistent with the loss of resolution with depth that is observed with all surface-based geophysical surveys.

The VOI results are very dependent on the automatic interpretation that was used to identify the clay throat location in every inversion (described in the Methodology Section). Interpretations are usually made by professionals with expertise in the technique and the particular location being imaged. Modifications could and should be made for specific applications.

We remind our readers that the objective of the study is to develop a VOI method that can evaluate spatial information from geophysical techniques, including the effects of 2D inversion. We chose to add complexity (sinter and increasing depths) to demonstrate the ability of the VOI methodology to incorporate geophysical limitations, including non-uniqueness, and lack of sensitivity and resolution. The slight asymmetry of clay cap first gave a slight bias to interpreting the location to the east of the actual location. This was further compounded when a sinter was added to the east, and when the depth of the target increased with increasing lateral location to the east. For real applications, the goal would be to represent the geologic structures deemed plausible (based on a priori information) for a particular exploration area.

The description of the prior uncertainty

Table 3 summarizes the three different V_{prior}'s calculated to demonstrate the role V_{prior} plays in the VOI assessment. It intuitively makes sense that with greater prior uncertainty (i.e. the uniform distribution), a new source of information such as electrical resistivity images computed from MT data will have more potential to provide value to decision-makers because the V_{prior} is lower (Figure 1). Our results confirmed this expectation.

However, this expectation is not a universal law. Sato (2011) summarizes some of the counterintuitive aspects of VOI, one being that VOI does not necessarily increase as the prior

uncertainty increases (Gould, 1974). Our intent when evaluating three possible prior uncertainty models (Figure 6) was to provide the reader with some intuition about the VOI metric. However, we do not claim nor was it our intent is to provide a comprehensive study of the relationship of the prior uncertainty and VOI.

The value outcomes (Figures 7 and 8)

The value outcomes represent the estimated gains and losses due to the combination of the true location of the clay cap and the choice of drilling location. The value outcomes of Figure 7 penalize drilling decisions that are ≥1,500m from the actual cap. In this situation, the value of perfect information will have more value when using this value outcome matrix versus that of Figure 8 since it can help us avoid costly outcomes. This is seen in Table 4. However, once the fallibility of the MT inversions are considered, the final VOI depends on both $V_{imperfect}$ and V_{prior}. As seen in Table 7, $VOI_{imperfect}$ is higher for the more forgiving value outcomes; this is because misinterpretations are punished less in this case. However, the largest V_{prior} occurs using a tighter Gaussian ***and*** the more forgiving value outcomes; therefore, $VOI_{imperfect}$ is higher for the less forgiving value outcomes for this prior uncertainty.

We have made an important assumption that the decision-maker is risk-neutral (not risk-adverse or risk-prone), thus assuming that the decision-maker's utility function is linear and the cash equivalent is equal to the expected value (Bratvold et al., 2009; Pratt, et al., 1995). More complicated risk-attitudes and preferences for certain decision alternatives could be incorporated. Again this is outside the scope of our study.

The strength of the relationship between a clay cap and an economic geothermal reservoir

Fundamental to the VOI paradigm is that the information source must be sensitive to the parameter that affects the outcome of the decision. The last set of results varied the probability of that clay cap presence is correlated with the existence of an economic geothermal resource. As expected, the smaller the probability of a resource existing below a clay cap (thus a smaller chance of a high-valued outcome), the lower the value of information. This prior probability should come from geologist, drilling engineer or another expert in the geothermal conditions of a particular locale.

For this example, VOI increases when the prior uncertainty is higher and the value outcomes decrease quickly for when one drills far from the target clay cap. It should be noted that these results are highly dependent on the framing of the decision problem. Here we focus on hidden resources and assume that a clay cap is indicative of a possible geothermal source. Many more geothermal possibilities could be included, such as a low-enthalpy system, in which there would be no clay cap.

Possible applications to current oil topics

Lastly, we like to remind readers of the broader topics that this methodology is applicable. An area where VOI could be useful is determining if ocean bottom nodes (OBN) provide significant improved efficacy versus the conventional 3D seismic survey. By evaluating the VOI of each, decision-makers could justify (or not) the significant cost increase for utilizing OBN.

VOI quantifies how relevant and reliable any particular information source is, given a decision with an uncertain outcome. VOI is a powerful technique that can be used to justify the costs of collecting the new, proposed data. We have provided a flexible framework that includes the spatial uncertainty in the decision and the information itself. This methodology can be applied to multiple subsurface resource decisions and geophysical techniques to assess the possible gain of knowledge.

Acknowledgements

The authors would like to thank John Ziagos for his early contributions to this work and the Geothermal Program of the Department of Energy for funding this research. This research was performed under the auspices of the U.S. Department of Energy by Lawrence Livermore National Laboratory under Contract No. DE-AC52-07NA27344.

References

Bhattacharjya, D., Eidsvik, J., & Mukerji, T. (2010). The value of information in spatial decision making. *Mathematical Geosciences*, *42*, 141–163.

Bratvold, R. B., Bickel, J. E., Risk, A., & Lohne, H. P. (2009). Value of Information in the Oil and Gas Industry : Past, Present, and Future. *PE Reservoir Evaluation & Engineering*, (August 2009), 11–14. doi:10.2118/110378-PA

Cumming, W. (2009). Geothermal resource conceptual models using surface exploration data. *PROCEEDINGS, Thirty-Fourth Workshop on Geothermal Reservoir Engineering* (p. SGP–TR–187). Stanford, California.

Eidsvik, J., Bhattacharjya, D., & Mukerji, T. (2008). Value of information of seismic amplitude and CSEM resistivity. *Geophysics*, *73*(4), R59–R69. doi:10.1190/1.2938084

Garg, S. K., Pritchett, J. W., Wannamaker, P. E., & Combs, J. (2007). Characterization of geothermal reservoirs with electrical surveys: Beowawe geothermal field. *Geothermics*, *36*(6), 487–517. doi:10.1016/j.geothermics.2007.07.005

Gould, J. (1974). Risk, Stochastic Preference, and the Value of Information. *Journal of Economic Theory*, *8*, 64–84.

Gunderson, R., Cumming, W., Astra, D., & Harvey, C. (2000). Analysis of smectite clays in geothermal drill cuttings by the methylene blue method : for well site geothermometry and resistivity sounding correlation. *Proceedings World Geothermal Congress* (pp. 1175–1181).

Houck, R. T. (2004). Predicting the economic impact of acquisition artifacts and noise. *The Leading Edge*, *23*(10), 1024–1031.

Houck, R. T. (2007). Time-lapse seismic repeatability—How much is enough? *The Leading Edge*, *26*(7), 828–834.

Houck, R. T., & Pavlov, D. A. (2006). Evaluating reconnaissance CSEM survey designs using Detection Theory. *The Leading Edge*, *25*, 994–1004.

Howard, R. A. (1966). Information Value Theory. *IEEE Transactions on Systems Science and Cybernetics*, *SSC-2*(1), 22–26.

IOM (Institute of Medicine). (2013). *Environmental Decisions in the Face of Uncertainty*. Washington, DC: The National Academies Press.

Karlsdóttir, R., Vilhjálmsson, A., Árnason, K., & Beyene, A. (2012). *Þeistareykir Geothermal Area , Northern Iceland 3D Inversion of MT and TEM Data* (p. 173). Reykjavík. Retrieved from www.isor.is

Key, K., & Ovall, J. (2011). A parallel goal-oriented adaptive finite element method for 2.5-D electromagnetic modelling. *Geophysical Journal International*, *186*(1), 137–154. doi:10.1111/j.1365-246X.2011.05025.x

Newman, G. A., Gasperikova, E., Hoversten, G. M., & Wannamaker, P. E. (2008). Three-dimensional magnetotelluric characterization of the Coso geothermal field. *Geothermics*, *37*(4), 369–399. doi:10.1016/j.geothermics.2008.02.006

Pinto, J. R., De Aguiar, J. C., & Moraes, F. S. (2011). The value of information from time-lapse seismic data. *The Leading Edge*, *30*(5), 572–576. doi:10.1190/1.3589116

Pratt, J., Raiffa, H., and Schlaifer, R. (1995). *Introduction To Statistical Decision Theory*. Cambridge, MA: The Massachusets Institute of Technology Press.

Raiffa, H. and Schlaifer, R. (1961). *Applied Statistical Decision Theory*. Cambridge, Massachusetts: Harvard University Press.

Richards, K., Revil, A., Jardani, A., Henderson, F., Batzle, M., & Haas, A. (2010). Pattern of shallow ground water flow at Mount Princeton Hot Springs , Colorado , using geoelectrical methods. *Journal of Volcanology and Geothermal Research*, *198*(1-2), 217–232. doi:10.1016/j.jvolgeores.2010.09.001

Sato, K. (2011). International Journal of Greenhouse Gas Control Value of information analysis for adequate monitoring of carbon dioxide storage in geological reservoirs under uncertainty. *International Journal of Greenhouse Gas Control*, *5*(5), 1294–1302. doi:10.1016/j.ijggc.2011.07.010

Trainor-Guitton, W. J., Caers, J. K., & Mukerji, T. (2011). A Methodology for Establishing a Data Reliability Measure for Value of Spatial Information Problems. *Mathematical Geosciences*, *43*(8), 929–949. doi:10.1007/s11004-011-9367-0

Trainor-Guitton, Whitney J., Mukerji, T., & Knight, R. (2013). A methodology for quantifying the value of spatial information for dynamic Earth problems. *Stochastic Environmental Research and Risk Assessment*, *27*(4), 969–983. doi:10.1007/s00477-012-0619-4

Trainor-Guitton, Whitney J., Ramirez, A., Yang, X., Mansoor, K., Sun, Y., & Carroll, S. (2013). Value of information methodology for assessing the ability of electrical resistivity to detect CO2/brine leakage into a shallow aquifer. *International Journal of Greenhouse Gas Control*, *18*, 101–113. doi:10.1016/j.ijggc.2013.06.018

Trainor-Guitton, Whitney Jane. (2010). *On the Value of Information for Spatial Problems in the Earth Sciences*. Stanford University.

Ucok, H., Ershaghi, I., & Olhoeft, G. (1980). 1980J Petrl Techn.pdf. *Journal of Petroleum Technology*, *32*, 717–727.

Wu, H., & Lees, J. M. (1999). Three-dimensional P and S wave velocity structures of the Coso Geothermal Area, California, from microseismic travel time data. *Journal of Geophysical Research, 104*(B6), 13,217–13,233.

Figure Captions

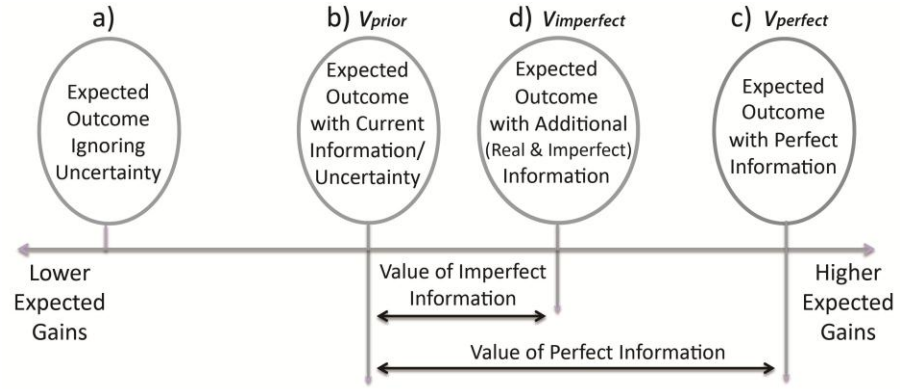

$$VOI = V_{with\ information} - V_{prior}$$

Figure 1: The outcome-uncertainty continuum that graphically represents the concepts behind VOI. Modified from: Institute of Medicine (2013).

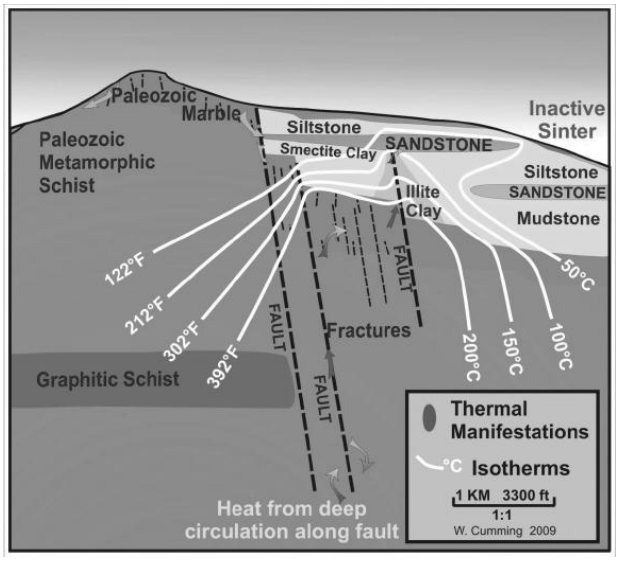

Figure 2: Conceptualization of blind geothermal resource where no surface feature exists to demonstrate existence of a possible resource (from Cummings 2009)

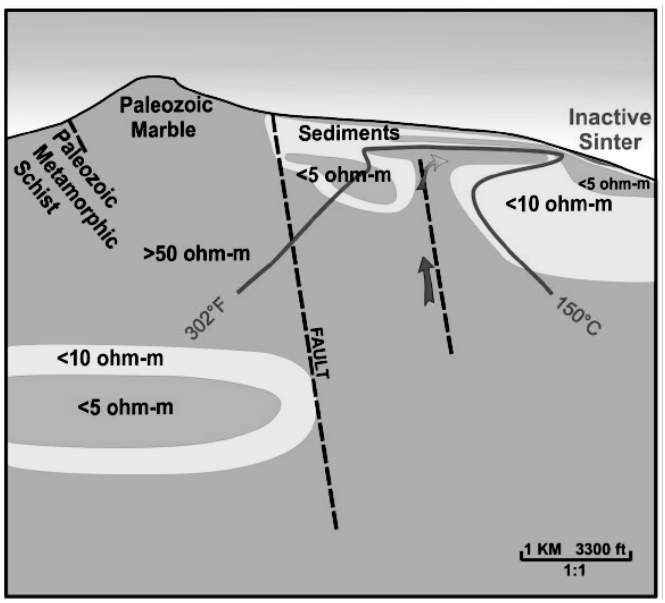

Figure 3: Conceptual model of electrical resistivity for a hidden geothermal resource (from Cumming, 2009)

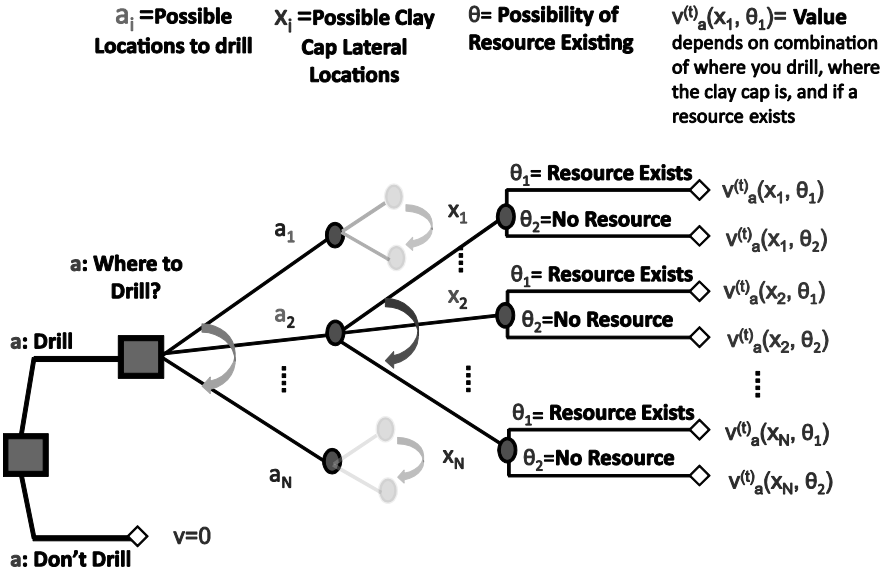

Figure 4: Decision tree where blue squares depict the spatial decision alternatives and the nodes depict both the uncertainty of the clay cap locations and the resource existence. Lastly, the unique combination of these alternatives and uncertainties result in an outcome measured in value (diamonds).

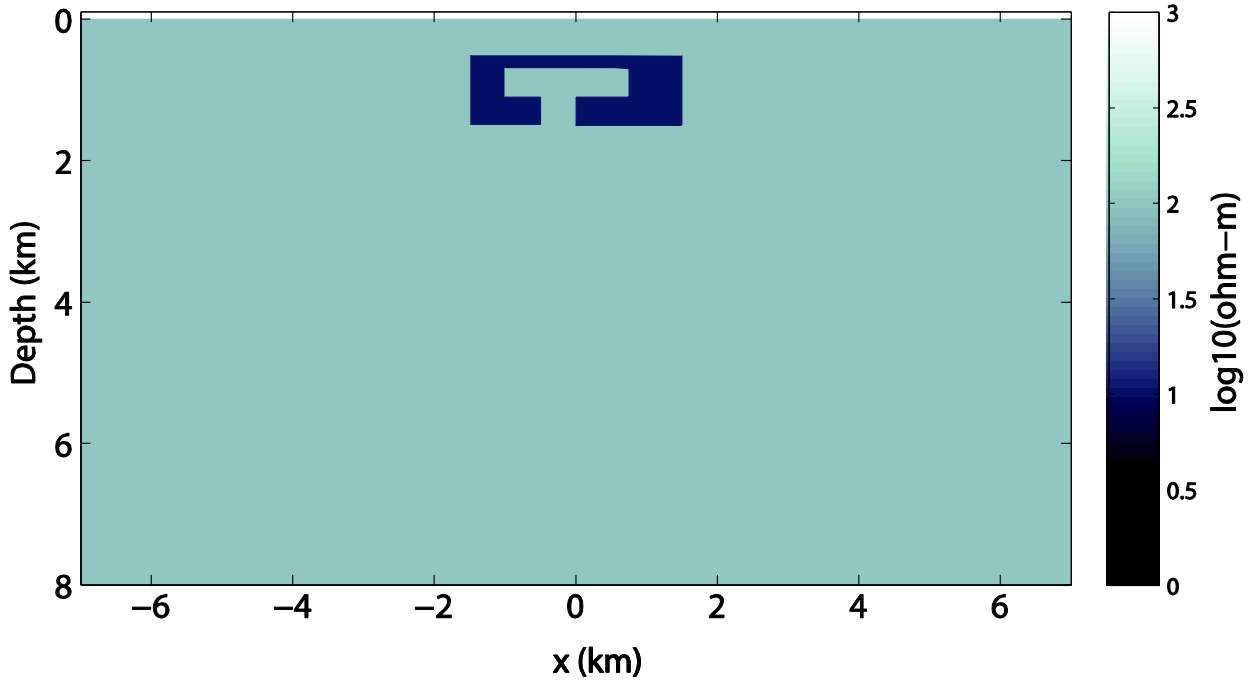

Figure 5: One realization of the electrical resistivity model representing the hidden resource. The dark grey cap represents the light grey 10 Ohm-m layer in Figure 3. The white layer is the air and the light grey is the background subsurface (100 Ohm-m).

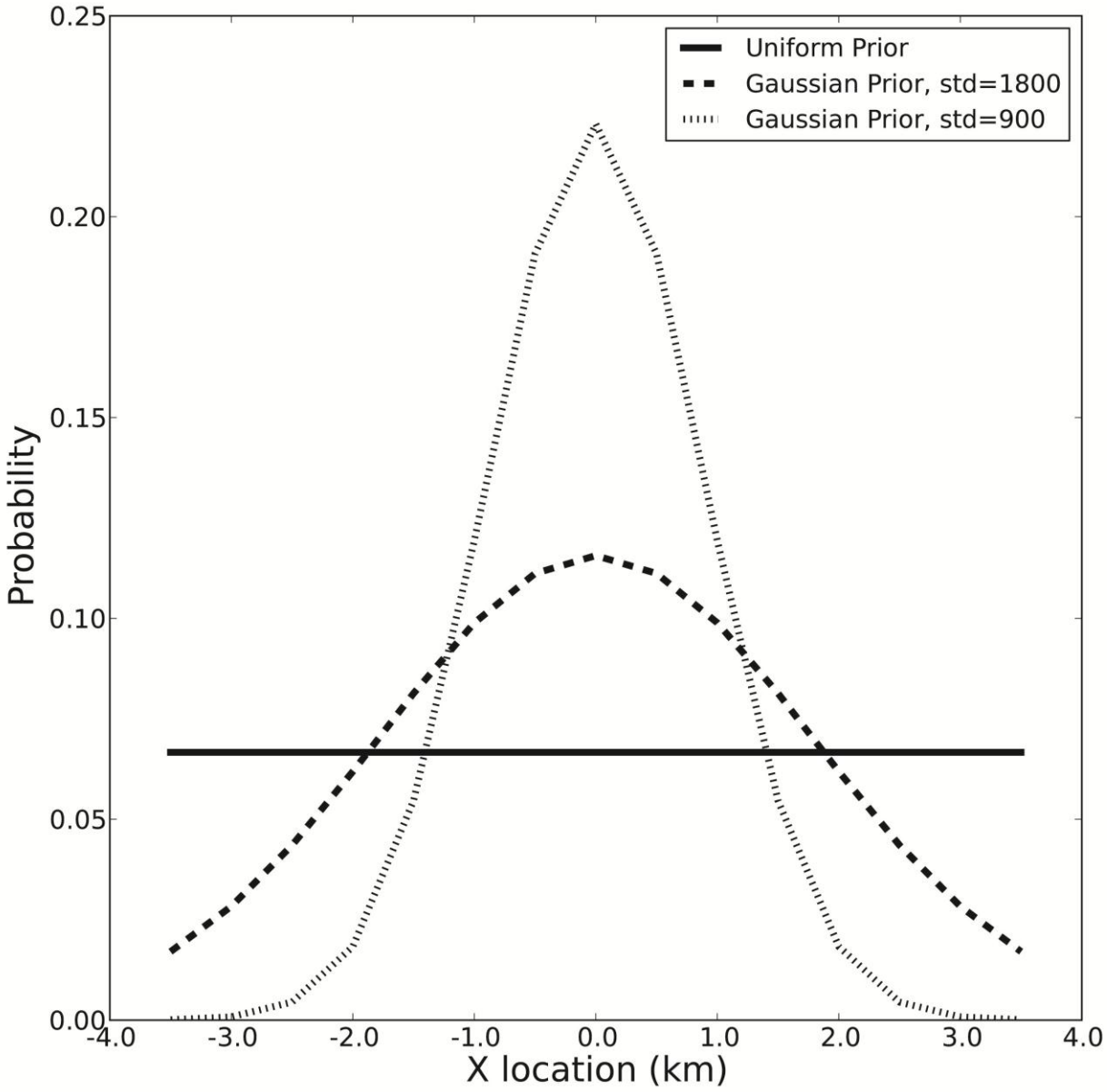

Figure 6: 3 Different Prior Distributions used to test Vprior sensitivity

	a1	a2	a3	a4	a5	a6	a7	a8	a9	a10	a11	a12	a13	a14	a15
x = -3500	$500,000	$200,000	$0	-$500,000	-$500,000	-$500,000	-$500,000	-$500,000	-$500,000	-$500,000	-$500,000	-$500,000	-$500,000	-$500,000	-$500,000
x = -3000	$200,000	$500,000	$200,000	$0	-$500,000	-$500,000	-$500,000	-$500,000	-$500,000	-$500,000	-$500,000	-$500,000	-$500,000	-$500,000	-$500,000
x = -2500	$0	$200,000	$500,000	$200,000	$0	-$500,000	-$500,000	-$500,000	-$500,000	-$500,000	-$500,000	-$500,000	-$500,000	-$500,000	-$500,000
x = -2000	-$500,000	$0	$200,000	$500,000	$200,000	$0	-$500,000	-$500,000	-$500,000	-$500,000	-$500,000	-$500,000	-$500,000	-$500,000	-$500,000
x = -1500	-$500,000	-$500,000	$0	$200,000	$500,000	$200,000	$0	-$500,000	-$500,000	-$500,000	-$500,000	-$500,000	-$500,000	-$500,000	-$500,000
x = -1000	-$500,000	-$500,000	-$500,000	$0	$200,000	$500,000	$200,000	$0	-$500,000	-$500,000	-$500,000	-$500,000	-$500,000	-$500,000	-$500,000
x = -500	-$500,000	-$500,000	-$500,000	-$500,000	$0	$200,000	$500,000	$200,000	$0	-$500,000	-$500,000	-$500,000	-$500,000	-$500,000	-$500,000
x = 0	-$500,000	-$500,000	-$500,000	-$500,000	-$500,000	$0	$200,000	$500,000	$200,000	$0	-$500,000	-$500,000	-$500,000	-$500,000	-$500,000
x = 500	-$500,000	-$500,000	-$500,000	-$500,000	-$500,000	-$500,000	$0	$200,000	$500,000	$200,000	$0	-$500,000	-$500,000	-$500,000	-$500,000
x = 1000	-$500,000	-$500,000	-$500,000	-$500,000	-$500,000	-$500,000	-$500,000	$0	$200,000	$500,000	$200,000	$0	-$500,000	-$500,000	-$500,000
x = 1500	-$500,000	-$500,000	-$500,000	-$500,000	-$500,000	-$500,000	-$500,000	-$500,000	$0	$200,000	$500,000	$200,000	$0	-$500,000	-$500,000
x = 2000	-$500,000	-$500,000	-$500,000	-$500,000	-$500,000	-$500,000	-$500,000	-$500,000	-$500,000	$0	$200,000	$500,000	$200,000	$0	-$500,000
x = 2500	-$500,000	-$500,000	-$500,000	-$500,000	-$500,000	-$500,000	-$500,000	-$500,000	-$500,000	-$500,000	$0	$200,000	$500,000	$200,000	$0
x = 3000	-$500,000	-$500,000	-$500,000	-$500,000	-$500,000	-$500,000	-$500,000	-$500,000	-$500,000	-$500,000	-$500,000	$0	$200,000	$500,000	$200,000
x = 3500	-$500,000	-$500,000	-$500,000	-$500,000	-$500,000	-$500,000	-$500,000	-$500,000	-$500,000	-$500,000	-$500,000	-$500,000	$0	$200,000	$500,000

Figure 7: Value outcomes that drop off quickly (i.e. losses are experienced when drilling ≥1,500m from actual clay cap). Rows represent the actual clay cap location and columns represent the drilling location (decision alternative). Lighter shades equals gain while darker shades equal loss.

	a1	a2	a3	a4	a5	a6	a7	a8	a9	a10	a11	a12	a13	a14	a15
x = -3500	$500,000	$366,000	$232,000	$98,000	-$500,000	-$500,000	-$500,000	-$500,000	-$500,000	-$500,000	-$500,000	-$500,000	-$500,000	-$500,000	-$500,000
x = -3000	$366,000	$500,000	$366,000	$232,000	$98,000	-$500,000	-$500,000	-$500,000	-$500,000	-$500,000	-$500,000	-$500,000	-$500,000	-$500,000	-$500,000
x = -2500	$232,000	$366,000	$500,000	$366,000	$232,000	$98,000	-$500,000	-$500,000	-$500,000	-$500,000	-$500,000	-$500,000	-$500,000	-$500,000	-$500,000
x = -2000	$98,000	$232,000	$366,000	$500,000	$366,000	$232,000	$98,000	-$500,000	-$500,000	-$500,000	-$500,000	-$500,000	-$500,000	-$500,000	-$500,000
x = -1500	-$500,000	$98,000	$232,000	$366,000	$500,000	$366,000	$232,000	$98,000	-$500,000	-$500,000	-$500,000	-$500,000	-$500,000	-$500,000	-$500,000
x = -1000	-$500,000	-$500,000	$98,000	$232,000	$366,000	$500,000	$366,000	$232,000	$98,000	-$500,000	-$500,000	-$500,000	-$500,000	-$500,000	-$500,000
x = -500	-$500,000	-$500,000	-$500,000	$98,000	$232,000	$366,000	$500,000	$366,000	$232,000	$98,000	-$500,000	-$500,000	-$500,000	-$500,000	-$500,000
x = 0	-$500,000	-$500,000	-$500,000	-$500,000	$98,000	$232,000	$366,000	$500,000	$366,000	$232,000	$98,000	-$500,000	-$500,000	-$500,000	-$500,000
x = 500	-$500,000	-$500,000	-$500,000	-$500,000	-$500,000	$98,000	$232,000	$366,000	$500,000	$366,000	$232,000	$98,000	-$500,000	-$500,000	-$500,000
x = 1000	-$500,000	-$500,000	-$500,000	-$500,000	-$500,000	-$500,000	$98,000	$232,000	$366,000	$500,000	$366,000	$232,000	$98,000	-$500,000	-$500,000
x = 1500	-$500,000	-$500,000	-$500,000	-$500,000	-$500,000	-$500,000	-$500,000	$98,000	$232,000	$366,000	$500,000	$366,000	$232,000	$98,000	-$500,000
x = 2000	-$500,000	-$500,000	-$500,000	-$500,000	-$500,000	-$500,000	-$500,000	-$500,000	$98,000	$232,000	$366,000	$500,000	$366,000	$232,000	$98,000
x = 2500	-$500,000	-$500,000	-$500,000	-$500,000	-$500,000	-$500,000	-$500,000	-$500,000	-$500,000	$98,000	$232,000	$366,000	$500,000	$366,000	$232,000
x = 3000	-$500,000	-$500,000	-$500,000	-$500,000	-$500,000	-$500,000	-$500,000	-$500,000	-$500,000	-$500,000	$98,000	$232,000	$366,000	$500,000	$366,000
x = 3500	-$500,000	-$500,000	-$500,000	-$500,000	-$500,000	-$500,000	-$500,000	-$500,000	-$500,000	-$500,000	-$500,000	$98,000	$232,000	$366,000	$500,000

Figure 8: Value outcomes that drop off more slowly (i.e. losses are only experienced when one drills ≥2,000m from the actual clay cap location). Rows represent the actual clay cap location and columns represent the drilling location (decision alternative). Lighter shades equal gain while darker shades equal loss.

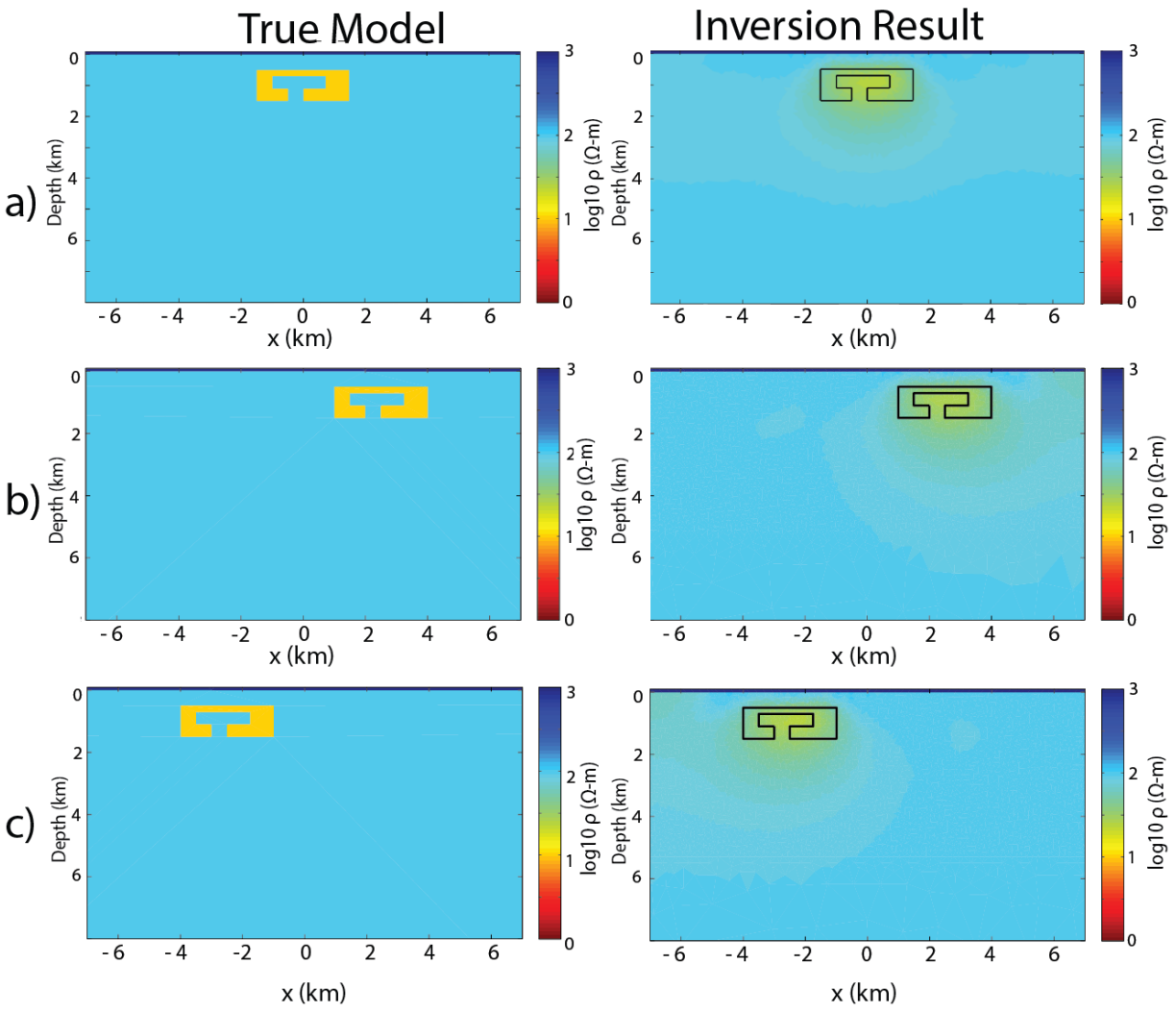

Figure 9: First column contains 3 prior models. The second column represents their respective inversion results. Clay cap located at a) x=0, b) x=+2500m and c) x=-2500m.

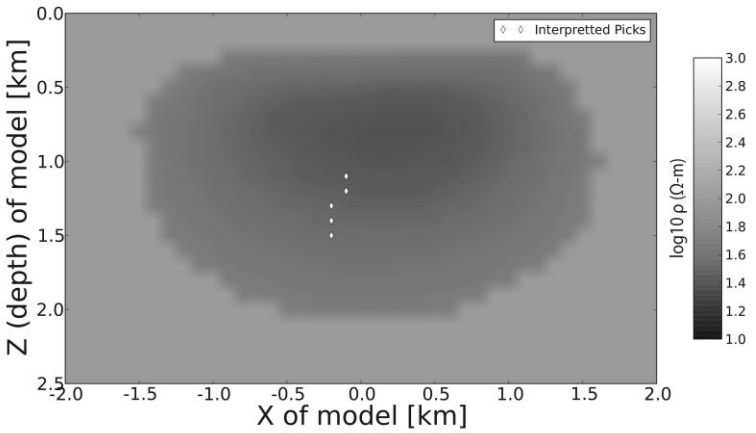

Figure 10: Example of interpreted lateral position (picks) at set depths = {1.1, 1.2, 1.3, 1.4, 1.5} km. The neck is interpreted to be at lateral locations within the warm color oval (rho < 10^1.7) that have the highest electrical resistivity. Example shown here corresponds to true clay cap neck at 0m, and the interpretations are between -500 and 0m. Notice different grey scale limits to better show resistivity.

	~x = -3500	~x = -3000	~x = -2500	~x = -2000	~x = -1500	~x = -1000	~x = -500	~x = 0	~x = 500	~x = 1000	~x = 1500	~x = 2000	~x = 2500	~x = 3000	~x = 3500
x = -3500	83.3%	0.0%	0.0%	0.0%	0.0%	0.0%	0.0%	0.0%	0.0%	0.0%	0.0%	0.0%	0.0%	0.0%	0.0%
x = -3000	16.7%	100.0%	26.1%	0.0%	0.0%	0.0%	0.0%	0.0%	0.0%	0.0%	0.0%	0.0%	0.0%	0.0%	0.0%
x = -2500	0.0%	0.0%	47.8%	50.0%	0.0%	0.0%	0.0%	0.0%	0.0%	0.0%	0.0%	0.0%	0.0%	0.0%	0.0%
x = -2000	0.0%	0.0%	26.1%	46.4%	23.1%	0.0%	0.0%	0.0%	0.0%	0.0%	0.0%	0.0%	0.0%	0.0%	0.0%
x = -1500	0.0%	0.0%	0.0%	3.6%	73.1%	0.0%	25.0%	0.0%	0.0%	0.0%	0.0%	0.0%	0.0%	0.0%	0.0%
x = -1000	0.0%	0.0%	0.0%	0.0%	3.8%	100.0%	5.0%	7.1%	0.0%	0.0%	0.0%	0.0%	0.0%	0.0%	0.0%
x = -500	0.0%	0.0%	0.0%	0.0%	0.0%	0.0%	70.0%	3.6%	76.9%	0.0%	0.0%	0.0%	0.0%	0.0%	0.0%
x = 0	0.0%	0.0%	0.0%	0.0%	0.0%	0.0%	0.0%	89.3%	0.0%	0.0%	0.0%	0.0%	0.0%	0.0%	0.0%
x = 500	0.0%	0.0%	0.0%	0.0%	0.0%	0.0%	0.0%	0.0%	23.1%	44.8%	37.5%	0.0%	0.0%	0.0%	0.0%
x = 1000	0.0%	0.0%	0.0%	0.0%	0.0%	0.0%	0.0%	0.0%	0.0%	55.2%	0.0%	31.0%	0.0%	0.0%	0.0%
x = 1500	0.0%	0.0%	0.0%	0.0%	0.0%	0.0%	0.0%	0.0%	0.0%	0.0%	62.5%	0.0%	62.5%	0.0%	0.0%
x = 2000	0.0%	0.0%	0.0%	0.0%	0.0%	0.0%	0.0%	0.0%	0.0%	0.0%	0.0%	69.0%	6.3%	21.1%	0.0%
x = 2500	0.0%	0.0%	0.0%	0.0%	0.0%	0.0%	0.0%	0.0%	0.0%	0.0%	0.0%	0.0%	18.8%	0.0%	40.0%
x = 3000	0.0%	0.0%	0.0%	0.0%	0.0%	0.0%	0.0%	0.0%	0.0%	0.0%	0.0%	0.0%	12.5%	78.9%	14.5%
x = 3500	0.0%	0.0%	0.0%	0.0%	0.0%	0.0%	0.0%	0.0%	0.0%	0.0%	0.0%	0.0%	0.0%	0.0%	45.5%

Figure 11: Information posterior for models with clay caps at 15 locations. Each row represents actual or true clay cap (prior model) and the columns represent how frequently that inverted clay cap was interpreted at different locations (represented by symbol ~x). Each column sums to 100%.

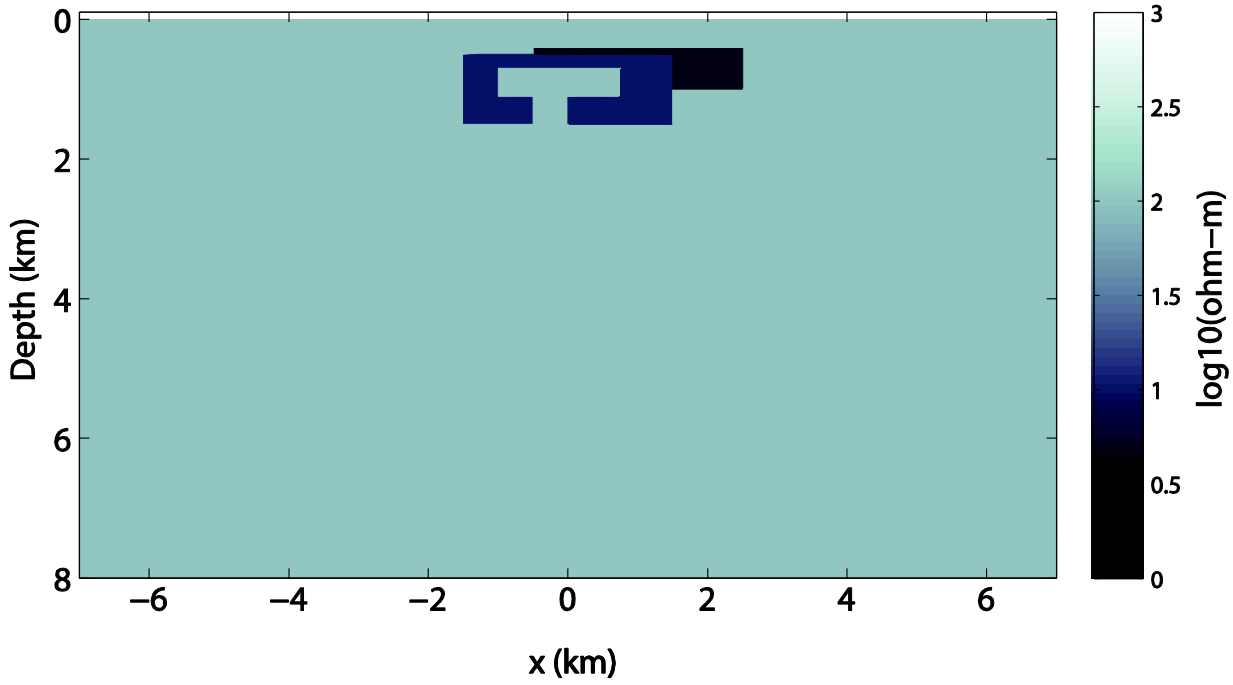

Figure 12: One realization of the electrical resistivity model representing the hidden resource (dark grey, 10 Ohm-m clay cap) with a sinter (represented in black, 5 Ohm-m color).

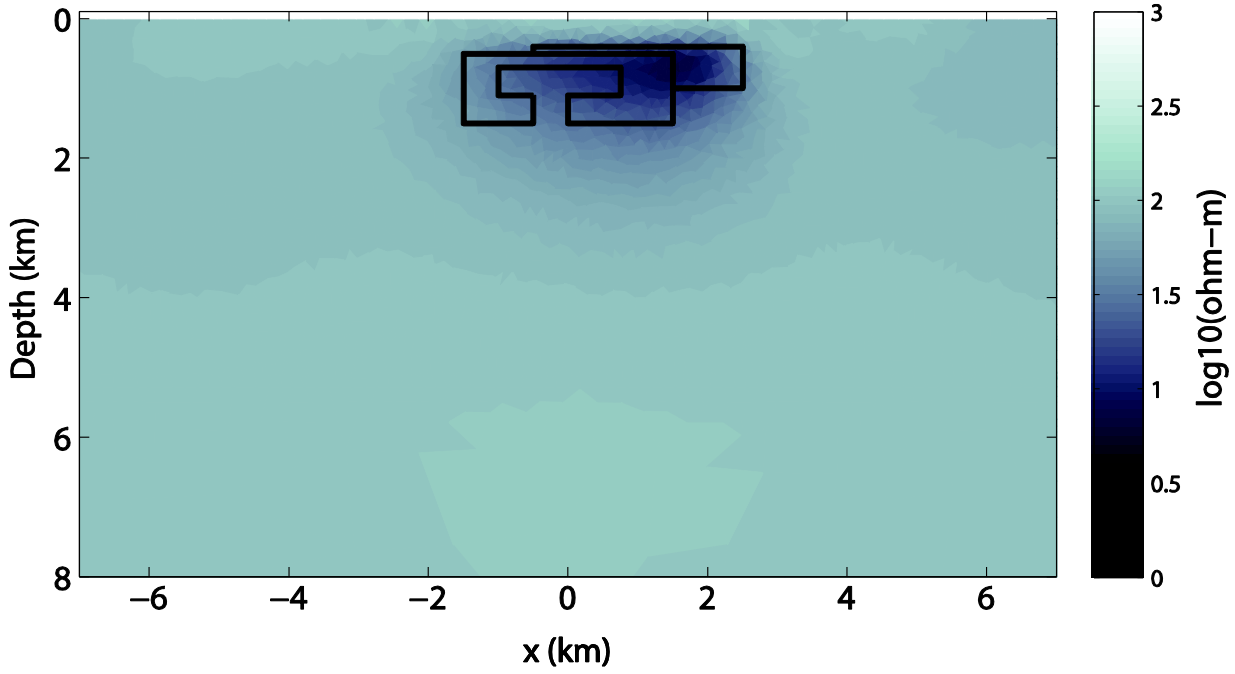

Figure 13: One inversion result from model shown in Figure 11 which includes a sinter. Outline of true locations of clay cap and sinter in black.

	~x = -3500	~x = -3000	~x = -2500	~x = -2000	~x = -1500	~x = -1000	~x = -500	~x = 0	~x = 500	~x = 1000	~x = 1500	~x = 2000	~x = 2500	~x = 3000	~x = 3500
x = -3500	100.0%	0.0%	41.7%	12.8%	0.0%	0.0%	0.0%	0.0%	0.0%	0.0%	0.0%	0.0%	0.0%	0.0%	0.0%
x = -3000	0.0%	0.0%	58.3%	28.2%	0.0%	0.0%	0.0%	0.0%	0.0%	0.0%	0.0%	0.0%	0.0%	0.0%	0.0%
x = -2500	0.0%	0.0%	0.0%	46.2%	41.2%	0.0%	0.0%	0.0%	0.0%	0.0%	0.0%	0.0%	0.0%	0.0%	0.0%
x = -2000	0.0%	0.0%	0.0%	12.8%	58.8%	44.4%	9.1%	0.0%	0.0%	0.0%	0.0%	0.0%	0.0%	0.0%	0.0%
x = -1500	0.0%	0.0%	0.0%	0.0%	0.0%	55.6%	68.2%	0.0%	0.0%	0.0%	0.0%	0.0%	0.0%	0.0%	0.0%
x = -1000	0.0%	0.0%	0.0%	0.0%	0.0%	0.0%	22.7%	50.0%	100.0%	0.0%	0.0%	0.0%	0.0%	0.0%	0.0%
x = -500	0.0%	0.0%	0.0%	0.0%	0.0%	0.0%	0.0%	50.0%	0.0%	23.8%	0.0%	0.0%	0.0%	0.0%	0.0%
x = 0	0.0%	0.0%	0.0%	0.0%	0.0%	0.0%	0.0%	0.0%	0.0%	45.2%	40.0%	0.0%	0.0%	0.0%	0.0%
x = 500	0.0%	0.0%	0.0%	0.0%	0.0%	0.0%	0.0%	0.0%	0.0%	31.0%	20.0%	42.9%	0.0%	0.0%	0.0%
x = 1000	0.0%	0.0%	0.0%	0.0%	0.0%	0.0%	0.0%	0.0%	0.0%	0.0%	40.0%	52.4%	22.9%	0.0%	0.0%
x = 1500	0.0%	0.0%	0.0%	0.0%	0.0%	0.0%	0.0%	0.0%	0.0%	0.0%	0.0%	4.8%	54.3%	22.7%	0.0%
x = 2000	0.0%	0.0%	0.0%	0.0%	0.0%	0.0%	0.0%	0.0%	0.0%	0.0%	0.0%	0.0%	22.9%	77.3%	0.0%
x = 2500	0.0%	0.0%	0.0%	0.0%	0.0%	0.0%	0.0%	0.0%	0.0%	0.0%	0.0%	0.0%	0.0%	0.0%	33.3%
x = 3000	0.0%	0.0%	0.0%	0.0%	0.0%	0.0%	0.0%	0.0%	0.0%	0.0%	0.0%	0.0%	0.0%	0.0%	33.3%
x = 3500	0.0%	0.0%	0.0%	0.0%	0.0%	0.0%	0.0%	0.0%	0.0%	0.0%	0.0%	0.0%	0.0%	0.0%	33.3%

Figure 14: Information posterior for models with clay caps and sinters at 15 locations. Each row represents actual or true clay cap (prior model) and the columns represent how frequently that inverted clay cap was interpreted at different locations (represented by symbol ~x).

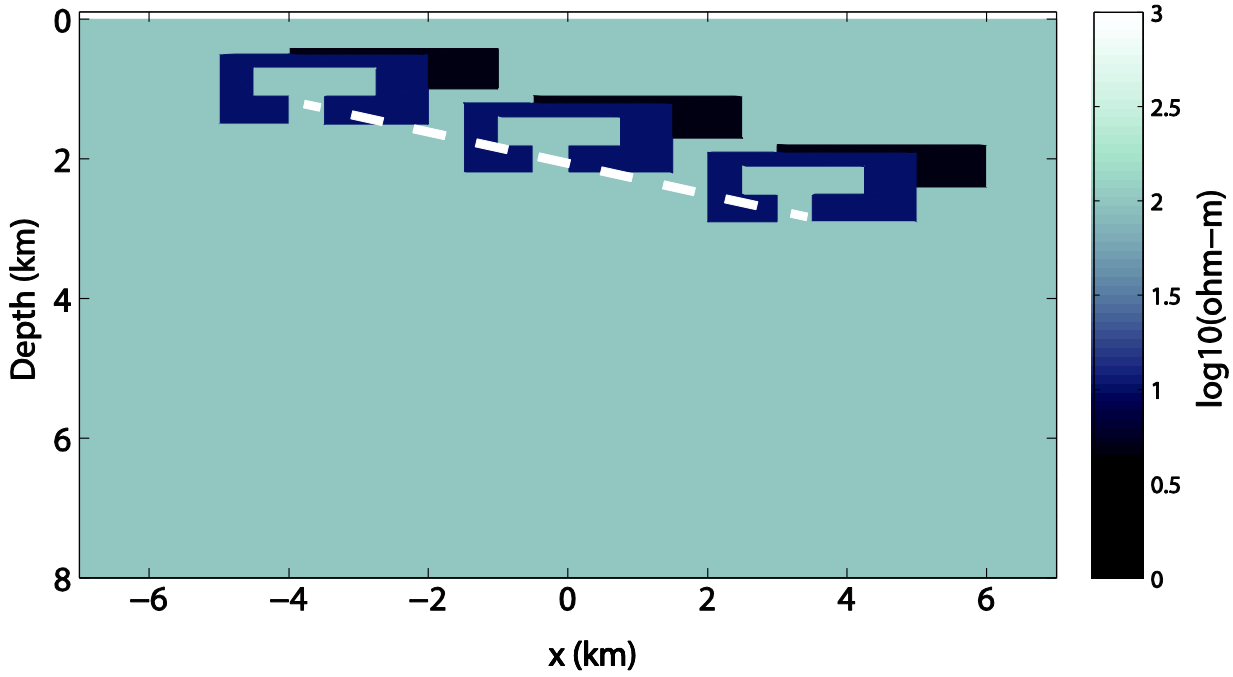

Figure 15: Schematic showing how the clay caps increase in depth with increasing eastern location.

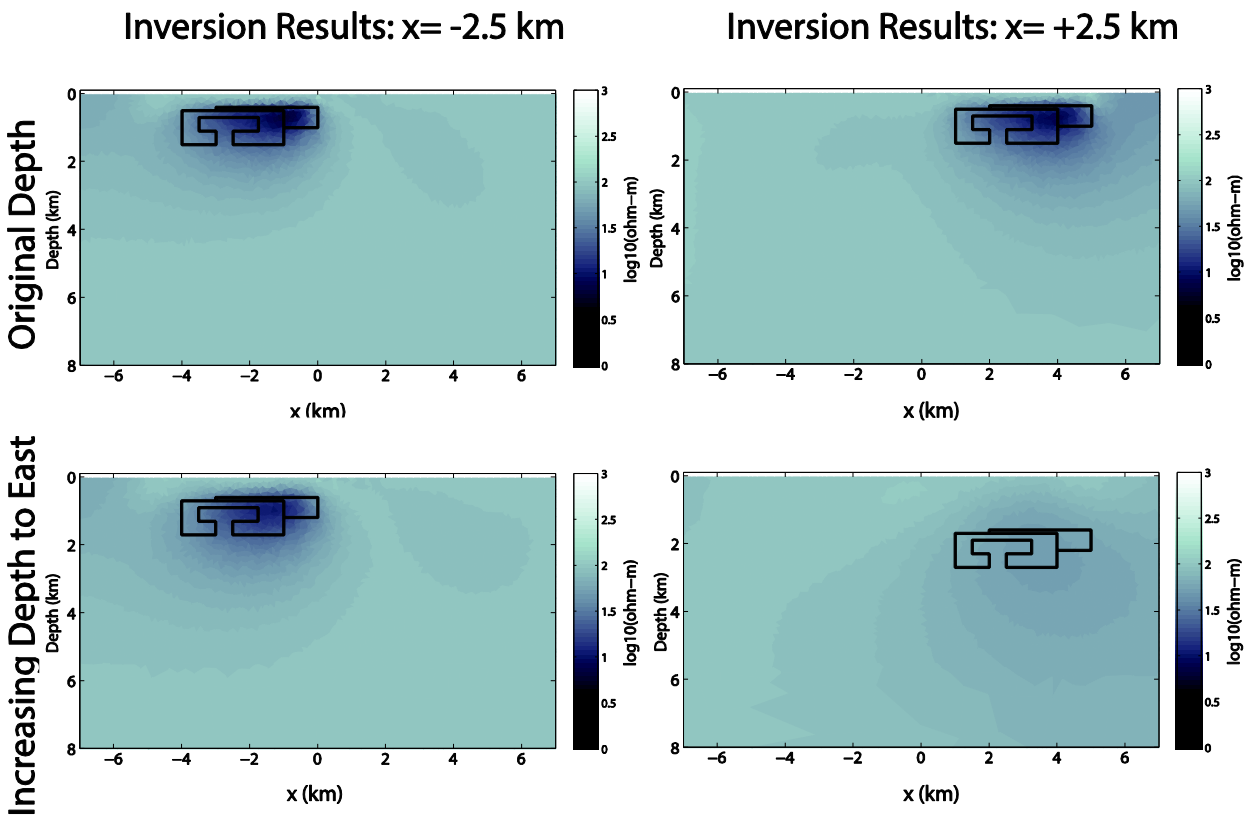

Figure 16: Inversion results for x=-2,500m (first column) and x=+2,500m (second column). The first row shows inversions where the clay caps are located at their original depths of 500 to 1000m. The bottom row shows inversions where the clay caps are located at greater depths: 200m and 1,200m deeper respectively.

	~x = -3500	~x = -3000	~x = -2500	~x = -2000	~x = -1500	~x = -1000	~x = -500	~x = 0	~x = 500	~x = 1000	~x = 1500	~x = 2000	~x = 2500	~x = 3000	~x = 3500
x = -3500	66.7%	0.0%	35.7%	14.3%	0.0%	0.0%	0.0%	0.0%	0.0%	0.0%	0.0%	0.0%	0.0%	0.0%	0.0%
x = -3000	0.0%	0.0%	46.4%	28.6%	8.3%	0.0%	0.0%	0.0%	0.0%	0.0%	0.0%	0.0%	0.0%	0.0%	0.0%
x = -2500	0.0%	0.0%	0.0%	42.9%	41.7%	0.0%	0.0%	0.0%	0.0%	0.0%	0.0%	0.0%	0.0%	0.0%	0.0%
x = -2000	0.0%	0.0%	0.0%	0.0%	29.2%	0.0%	45.0%	0.0%	0.0%	0.0%	0.0%	0.0%	0.0%	0.0%	0.0%
x = -1500	0.0%	0.0%	0.0%	0.0%	0.0%	77.3%	5.0%	14.3%	0.0%	0.0%	0.0%	0.0%	0.0%	0.0%	0.0%
x = -1000	0.0%	0.0%	0.0%	0.0%	0.0%	0.0%	37.5%	0.0%	22.2%	0.0%	0.0%	0.0%	0.0%	0.0%	0.0%
x = -500	0.0%	0.0%	0.0%	0.0%	0.0%	0.0%	0.0%	38.1%	0.0%	39.1%	0.0%	0.0%	0.0%	0.0%	0.0%
x = 0	0.0%	0.0%	0.0%	0.0%	0.0%	0.0%	0.0%	23.8%	11.1%	0.0%	58.3%	18.8%	0.0%	0.0%	0.0%
x = 500	0.0%	0.0%	0.0%	0.0%	0.0%	0.0%	0.0%	11.9%	42.2%	4.3%	0.0%	0.0%	0.0%	0.0%	0.0%
x = 1000	0.0%	0.0%	0.0%	0.0%	0.0%	0.0%	0.0%	0.0%	13.3%	13.0%	0.0%	0.0%	0.0%	44.4%	22.2%
x = 1500	0.0%	0.0%	0.0%	0.0%	0.0%	0.0%	0.0%	0.0%	0.0%	21.7%	0.0%	0.0%	0.0%	0.0%	37.0%
x = 2000	0.0%	0.0%	0.0%	0.0%	0.0%	0.0%	0.0%	0.0%	0.0%	0.0%	0.0%	50.0%	0.0%	0.0%	31.5%
x = 2500	11.1%	33.3%	6.0%	4.8%	6.9%	7.6%	4.2%	4.0%	3.7%	7.2%	13.9%	10.4%	33.3%	18.5%	3.1%
x = 3000	11.1%	33.3%	6.0%	4.8%	6.9%	7.6%	4.2%	4.0%	3.7%	7.2%	13.9%	10.4%	33.3%	18.5%	3.1%
x = 3500	11.1%	33.3%	6.0%	4.8%	6.9%	7.6%	4.2%	4.0%	3.7%	7.2%	13.9%	10.4%	33.3%	18.5%	3.1%

Figure 17: Information Posterior for models dipping with eastern lateral location of the clay cap and sinter.